2014 IEEE International Conference on Robotics & Automation (ICRA)
Hong Kong Convention and Exhibition Center
May 31 - June 7, 2014. Hong Kong, China

Robotic Assistance for Manipulating a Flexible Endoscope*

L. A. Zhang, *Student member, IEEE*, R. Khare, E. Wilson, S. X. Wang, C. A. Peters, K. Cleary

***Abstract*—Flexible ureteroscopes are widely used for inspection, access, and manipulation in the ureter and kidney during uretero-renoscopy. However, existing endoscope designs rely on decades-old manual controls for translation, rotation, and tip flexion. The development of a more intuitive and user-friendly control system has the potential to greatly enhance the safety, efficacy, and efficiency of endoscopic procedures. Based on a first generation prototype, our lab designed an ergonomically enhanced flexible endoscopy robotic system. The system was designed to enable the surgeon to operate the endoscope through a low cost game controller. The kinematics were analyzed considering the nonlinearity of flexion driving and cable slack. The kinematics control was combined with the direct control for the system. The initial evaluations show the feasibility of this approach.**

I. Introduction

Flexible endoscopy is commonly performed in all aspects of medicine including ureteroscopy, colonoscopy, etc. Uretero-renoscopy is used widely for stone removal, diagnosis for bleeding or malignancy, as well as direct biopsy and destruction of malignant lesions. In stone disease, ureteroscopy is becoming more widely used than the other minimally invasive means to remove stones in both adults and children [1]. However, existing endoscope designs are based on decades-old manual controls for translation, rotation and tip flexion. The ergonomics are poor, for instance, it can be hard to turn the control dials for surgeons who perform the procedure without an assistant [2]. Flexible endoscopes are not easy to stabilize [3] especially when the procedure requires holding the endoscope for a long time. Because of the complexity of movements needed for many applications, integration of a more intuitive and user-friendly control system has the potential to greatly enhance the safety, efficacy, and efficiency of these instruments.

Robotic systems present a promising avenue to address the challenges in conventional endoscopy. In related work, researchers at Johns Hopkins developed robotic assistance for a flexible endolaryngoscope [4]. This robot was controlled by a SpaceNavigator 3D mouse (3D Connexion, Rochester, MI). We have also previously designed and fabricated a first generation prototype that is remotely controlled by a 3D mouse for robotically assisted ureteroscopy [5]. However, these devices do not provide a fast mechanism for securing and removing the endoscope, thus, leading to a disrupted clinical workflow. Desai et al. have used the flexible Sensei robotic catheter system for renal calculi in 18 patients [6]. Other researchers developed a steerable robot driven by two remote motors through Bowden cables which is compact but its translation movement is manually controlled [7]. Guo has integrated force sensors to get force information from the tip of the catheter [8]. Chen has developed a motorized hand-held flexible rhino endoscope for ENT inspection [9]. The flexion and rotation of the endoscope is driven by motors but the translation is controlled by hand. Yoon has compensated for bending error by measuring the actual pose of the flexible endoscope [10].

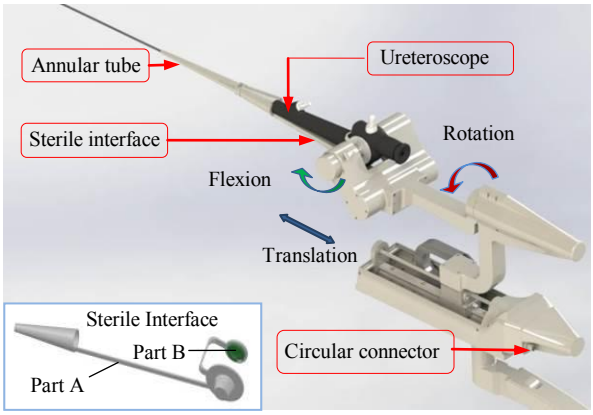

Figure 1. Second generation of ureteroscopic robot

The main contribution of this paper is in presenting a ureteroscopic robot which is ultimately intended for clinical use. As shown in Fig. 1, the robotic system makes it easy for a surgeon to snap-in and remove the ureteroscope in a sterile manner. Design objectives are presented with a comprehensive model of kinematics and the surgeon's intuitive operating experience. The velocity control by combining kinematics and direct control mode is designed for the robot and some experiments are presented to test the performance of the robot.

II. Design Specification

A. Workflow

The robotic system that we have designed is intended to enhance the existing workflow for ureteroscopy. In this workflow, the access to the renal pelvis is obtained manually following current clinical practice, since access is typically not difficult. Then, the ureteroscope is wrapped up in a sterile interface and snapped into the mechanical drive system, which will be located between the legs of the patient. From

* Children's National Medical Center work is supported by the Sheikh Zayed Institute, funded by a gift from the government of Abu Dhabi. Tianjin University work is supported by Chinese Scholarship Council under grant scholarship No. 201206250043 and NSFC fund 51375494.

The authors are with Sheikh Zayed Institute for Pediatric Surgical Innovation, Children's National Medical Center, Washington DC 20010 USA (phone: 202-476-3809; fax: 202-476-1270; e-mail: kcleary@cnmc.org).

L. A. Zhang and S. X. Wang are also with Tianjin University, Tianjin, 300072 China. (e-mail: zla3452@tju.edu.cn).

this point, the physician will be able to manipulate the utereroscope using the control system described in this paper.

B. Clinical Experiences and Requirements

As a surgical device, in addition to feasibility, the ureteroscopic robot should also focus on usability, safety and ergonomic performance. We decided on the following design criteria for our prototype: (1) endoscopist can quickly and efficiently mount the endoscope on the robot; (2) the design should facilitate a sterile interface between the ureteroscope and the robot to prevent contamination; (3) the robot design should increase the stiffness of the flexible portion of the ureteroscope for improved maneuverability; (4) robotic motor cables should be routed properly to avoid tangling with the light and video cables, and prevent cable breaks due to robot motion; and (5) the robotic system is designed to work with existing commercial ureteroscopes.

C. Mechanical Design

The second generation prototype robot has three degrees of freedom as shown in Fig. 1. The ureteroscope used for this design is a Richard Wolf ureteroscope (Richard Wolf Medical Instrument Corp., Vernon Hills, IL, USA). The ureteroscope is mounted on the robot so that each motor independently manipulates rotation, flexion, and insertion (translation) of the ureteroscope. Three Maxon brushless motors (ECmax16 8W) with encoders (MR 512 counts per turn) and three Maxon gear boxes (two GP22C 690:1 reduction ratio for the rotation and flexion and one GP22C 84:1 reduction ratio for translation) are used to drive the joints. Limit switches are installed for each joint as a safety measure to prevent excessive travel for each joint. The translation motion is realized by combining a ball screw and guide rails.

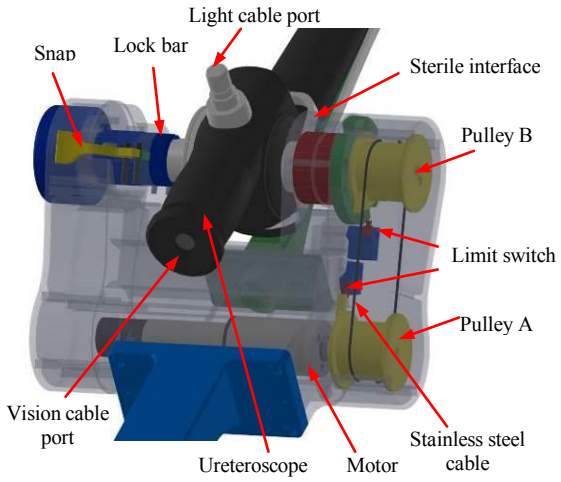

Figure 2. 3D model of fast snap-on mechanism to secure the ureteroscope and mechanism to drive tip flexion.

The mounting mechanism is shown in Fig. 2. A sterile interface piece (bottom left of Fig. 1) is placed on the ureteroscope before it is mounted on the robot. One side of the sterile interface with a flat shaft is inserted into a hole in the drive shaft, which is fixed to the pulley B. Stainless wire with the diameter of 0.87 mm was used to transmit motion from the pulley A to the pulley B. The other side of the sterile interface is cone shaped and fixed in place by pushing tightly into a lock bar.

Fig. 3 shows the fast snap-on mechanism to secure the ureteroscope. When the endoscopist presses the push button, lock teeth slide into the groove of the lock bar. Two snaps located on both sides of the lock bar secure the lock teeth in position. Thus, the ureteroscope is tightly fixed on the robot. The snaps are always open under the force of the bending springs. When the snaps are pushed in, pulling springs pull back the lock bar, thus releasing the sterile interface. This design makes it easy to install and uninstall the endoscope.

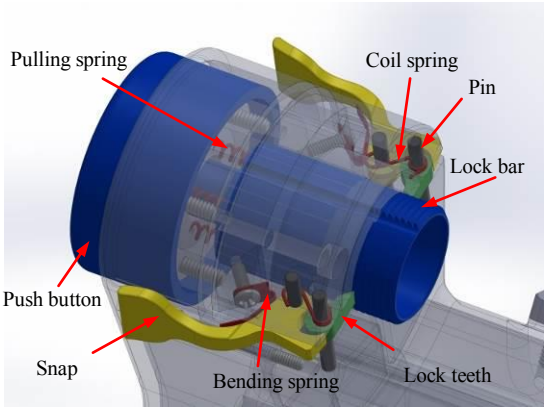

Figure 3. Detailed view of snap-on mechanism.

Since the ureteroscope consists of a long flexible cable that is inserted into the body, the part of the cable between the robot and the body may sag which is not desirable. Therefore, we created a rigid annular tube with higher stiffness to support the ureteroscope shaft during insertion. The length of the tube can be modified as needed to fit different endoscopes.

Because the light cable and vision cable of the ureteroscope are usually perpendicular to each other, these cables may become tangled with the motor cables when moving the rotation joint. This would happen frequently with the first generation prototype because in that design the motor and encoder cables from the robot are routed with the vision cable. In the new design, all the motor and encoder cables are internally routed to avoid interference and terminated with two circular connectors at the bottom.

TABLE I. SPECIFICATIONS OF THE DESIGNED ROBOT

Range of motion	***Translation***	170 mm
	Rotation	±150°
	Flexion	~45°
Maximum driving torque	***Translation***	0.4 N/m
	Rotation	2.7 N/m
	Flexion	2.7 N/m
Weight		3.8 Kg

The overall robot design is also ergonomically improved compared to the first generation robot. Most of the parts were made on a 3D printer (Objet 500). The ABS material used makes the robot very light. A commercial supporting arm

with three joints is used to support the robot. Table 1 contains some general specifications of the robot. Note that while the robot's control dials for flexion only rotates about 45 degrees, this is mapped to the tip flexion of the scope of 270 degrees.

III. KINEMATICS

Fig. 4 depicts the tip of the ureteroscope. This end of the ureteroscope is mounted on the robot and is driven with three degrees of freedom. We denote the rotation of the ureteroscope about its axis by θ_2, and translation by d_3. A bending knob on the remote proximal end is internally connected to a pair of opposing pull wires to actuate flexion of the ureteroscope tip as shown in Fig. 4 (b). The rotation of this bending knob is denoted by θ_1. To formulate the expression for ureteroscope kinematics, we consider three frames of reference. The first frame of reference is a co-ordinate frame (X-Y-Z) fixed at the distal-most end of the ureteroscope that does not flex. The second frame of reference is a co-ordinate frame (x-y-z) fixed at the ureteroscope tip. The rotation and translation of the X-Y-Z co-ordinate axis is identical to that of the ureteroscope. To explain the flexion angle α, we consider the point O of intersection of the tangent to the ureteroscope tip and the Y axis. The flexion angle is defined as the angle subtended by the flexion segment of the ureteroscope at the point O. The flexion angle α is not equal to θ_1. Several kinematic strategies focused on positioning of flexible tool such as flexible instrument, and catheter have already been developed [11, 12]. We will use these techniques as the basis of our approach to control the ureteroscopic robot.

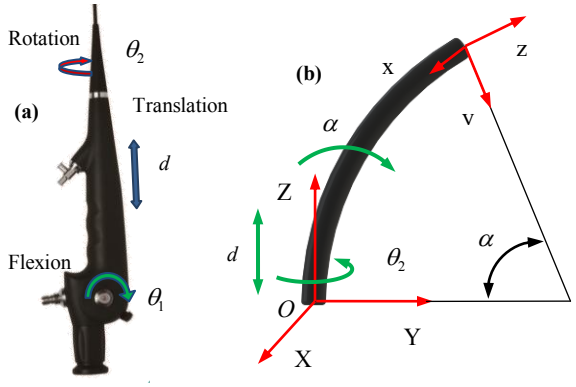

Figure 4. Actuated degrees of freedom and kinematic geometry of ureteroscope. (a) actuated degrees of freedom; (b) kinematic geometry

A. Ureteroscope Flexion

Many studies have introduced the kinematics of flexible endoscopes or other instruments [13]. The kinematic model in this paper is based on combining the geometric principles and classic robot kinematics [14]. We derived closed-form kinematic solutions for the forward kinematics, inverse kinematics, and velocity analysis. Similar work has been done previously, however this work assumed that the catheter bends with a constant radius of curvature [11]. For ureteroscope, the radius of curvature of the flexion segment changes with the flexion angle α.

Moreover, the flexion toward clockwise and anticlockwise direction is not linear with respect to the first handle input θ_1. Instead, the curve relating α and θ_1 for the two directions are offset by a small amount as shown in Fig. 5. This is because of a "dead zone" due to slack in the pull wire strings and a lack of tension when the bending knob crosses the zero position. By estimating the curves relating the flexion angle α and the bending knob angle θ_1, we can compensate for the "dead zone" effect. This estimation also allows us to estimate the non-linear mechanism of the pull strings that actuate the flexion. One issue is that different flexible endoscopes may have different curves, so the system would need re-calibration before we use a new endoscope.

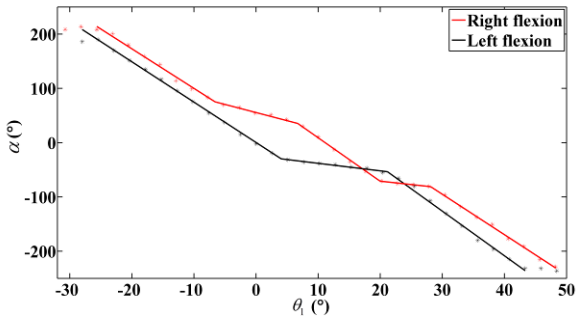

Figure 5. Tip flexion angle α as function of the bending knob angle θ_1

B. Forward Kinematics

As shown in Fig. 5, piecewise functions are used to estimate the two curves. Each section is fitted to a line. When the ureteroscope is bent toward anticlockwise direction, the flexion is divided into five segments.

$$\alpha = k_i^L \theta_1 + b_i^L \quad (i = 1,\ 2,\ ...,\ 5) \tag{1}$$

and when the ureteroscope is bent toward clockwise direction, the flexion is divided into 3 segments.

$$\alpha = k_i^R \theta_1 + b_i^R \quad (i = 1,\ 2,\ 3) \tag{2}$$

The forward kinematics model uses the inputs of the ureteroscope θ_1, θ_2 and d_3 to calculate the position and orientation at the ureteroscope tip. The length of bending section, L, must be known as well. According to the kinematic model of Fig. 4, the radius of curvature is

$$R = L/\alpha \tag{3}$$

The position of ureteroscope tip in X-Y-Z co-ordinates can be calculated using R and α when the translation and rotation are not taken into consideration. The position is

$$P_x^F = 0 \tag{4}$$

$$P_y^F = R(1 - \cos\alpha) \tag{5}$$

$$P_z^F = R\sin\alpha \tag{6}$$

The tip orientation due to bending can be calculated by applying a transformation which rotates the orientation by angle α about the X-axis. This transformation is given by

$$T_{Flex}(\alpha)=\begin{bmatrix}1 & 0 & 0 & P_x^F\\ 0 & \cos\alpha & -\sin\alpha & P_y^F\\ 0 & \sin\alpha & \cos\alpha & P_z^F\\ 0 & 0 & 0 & 1\end{bmatrix} \quad (7)$$

The transformation matrixes of rotation and translation are $T_{Rot}(\theta_2)$ and $T_{Trans}(d_3)$. Therefore the forward kinematics transformation matrix is

$$T_{Tip}=T_{Trans}(d_3)T_{Rot}(\theta_2)T_{Flex}(\theta_1,\ \alpha)=\begin{bmatrix}R_{3\times3} & \mathbf{P}_{Tip}\\ \mathbf{0} & 1\end{bmatrix} \quad (8)$$

where $C\theta_2$ and $S\theta_2$ denote $\cos\theta_2$ and $\sin\theta_2$, respectively and $C\alpha$ and $S\alpha$ denote $\cos\alpha$ and $\sin\alpha$, respectively.

$$R_{3\times3}=\begin{bmatrix}C\theta_2 & -S\theta_2C\alpha & S\theta_2S\alpha\\ S\theta_2 & C\theta_2C\alpha & -C\theta_2S\alpha\\ 0 & S\alpha & C\alpha\end{bmatrix} \quad (9)$$

$$\mathbf{P}_{Tip}=\begin{bmatrix}P_x^FC\theta_2-P_y^FS\theta_2 & P_x^FS\theta_2+P_y^FC\theta_2 & P_z^F+d_3\end{bmatrix}^T \quad (10)$$

C. Inverse Kinematics

The inverse kinematic model takes the ureteroscope tip position and orientation matrix, T_{Tip}, as input and solves for the single possible ureteroscope configuration. The model outputs the required joint angles required to achieve the desired configuration. It is possible to solve for intermediate variables α and R. Calculating the dot product of the world z-axis in X-Y-Z coordinate system and the ureteroscope tip z-axis in x-y-z coordinate system defines the angle α.

$$\alpha=\cos^{-1}\left(Z^{World}\bullet Z^{Tip}\right) \quad (11)$$

The flexion input angle θ_1 can be calculated according to the equation (1) and (2).

$$\theta_1=\begin{cases}\dfrac{\alpha-b_i^L}{k_i^L} & (i=1,\ 2,\ \cdots,\ 5), \quad \text{Right flexion}\\ \dfrac{\alpha-b_i^R}{k_i^R} & (i=1,\ 2,\ 3), \quad \text{Left flexion}\end{cases} \quad (12)$$

Given the ureteroscope tip position $P_{Tip}\begin{pmatrix}P_x & P_y & P_z\end{pmatrix}$, we substitute equation (3) - (6) into (10). Thus the two other inputs θ_2 and d_3 can be obtained.

$$\theta_2=\cos^{-1}\left(\frac{P_y}{R(1-\cos\alpha)}\right) \quad (13)$$

$$d_3=P_z-R\sin\theta_2 \quad (14)$$

D. Velocity Analysis

We use the velocity control to move the ureteroscopic robot. For this control, the velocity of the driving joints should be calculated. Before calculating the joint velocity by using the joystick, the joystick velocity $V_{Joystick}\begin{pmatrix}V_x^{Joy} & V_y^{Joy} & V_z^{Joy}\end{pmatrix}$ in joystick coordinate system should be mapped into the velocity $V_{Tip}\begin{pmatrix}V_x & V_y & V_z\end{pmatrix}$ in the X-Y-Z coordinate system.

$$\mathbf{V}_{Tip}=\begin{bmatrix}V_x\\ V_y\\ V_z\end{bmatrix}=-k_cR_{3\times3}\begin{bmatrix}V_x^{Joy}\\ V_y^{Joy}\\ V_z^{Joy}\end{bmatrix} \quad (15)$$

where k_c is a scalefactor. The velocity can be obtained by differentiating equation (10).

$$\begin{bmatrix}V_x\\ V_y\\ V_z\end{bmatrix}=\begin{bmatrix}-RS\alpha S\theta_2 & -R(1-C\alpha)C\theta_2 & 0\\ RS\alpha C\theta_2 & -R(1-C\alpha)S\theta_2 & 0\\ RC\alpha & 0 & 1\end{bmatrix}\begin{bmatrix}\dot\alpha\\ \dot\theta_2\\ \dot d_3\end{bmatrix} \quad (16)$$

The robotic motion contains two types of motion, rotation and translation. Considering the rotation part first, the velocity Jacobian matrix for the rotation part according to equation (16) is

$$J_{Rot}=\begin{bmatrix}-RS\alpha S\theta_2 & -R(1-C\alpha)C\theta_2\\ RS\alpha C\theta_2 & -R(1-C\alpha)S\theta_2\end{bmatrix} \quad (17)$$

From equation (17), the angular velocities of the two rotational joints can be calculated using

$$\begin{bmatrix}\dot\alpha\\ \dot\theta_2\end{bmatrix}=J_{Rot}^{-1}\begin{bmatrix}V_x\\ V_y\end{bmatrix} \quad (18)$$

The translation velocity is also obtained by differentiating the third element of the tip position $\mathbf{P}_{Tip}$ in equation (10).

$$\dot d_3=V_z-\dot\alpha R\cos\alpha \quad (19)$$

IV. Control

A. Controller Architecture

The architecture of the overall system is shown in Fig. 6. The robotic framework is interfaced to a computer through a Galil motion controller DMC-4133 (Galil Motion Control, Rocklin, CA, USA). The motion controller connects to a host computer by a USB or 100BASE-T Ethernet port. Four 750W servo drives are integrated on the Galil controller board. The Galil application programming interface is used to control the robotic framework. A low cost and light game controller serves as the user interface device and is also connected to the computer. This control framework allows the physician to more ergonomically control the ureteroscope while comfortably seated. The input from the user interface devices is converted into control signals by the interfacing software to

drive the robotic framework. This software included modules to evaluate the operative efficiency and accuracy of the robot system. The software was implemented as a dialog-based MFC application in Visual C++ on the Windows operating system.

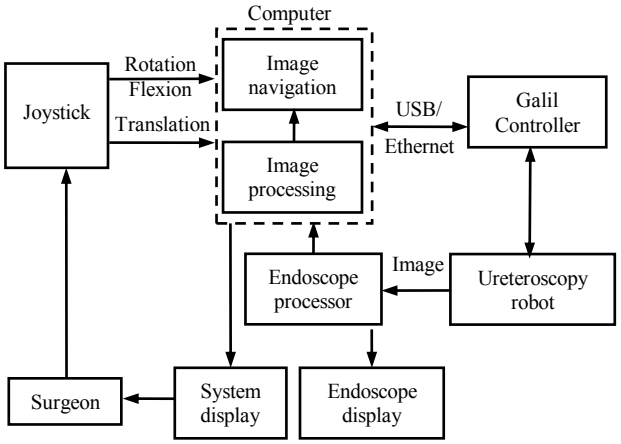

Figure 6. Block diagram of overall system including controller

B. Control Strategy

Since the ureteroscope has just one bending DOF, it is very difficult to move the ureteroscope along an axis which is perpendicular with the bending plane. The condition number of the Jacobian matrix of the robot changes with the handle input θ_1 and θ_2 is shown in Fig. 7 [12]. The robot has a low kinematic performance when the first handle input θ_1 is around home position. For high efficiency, this condition must be avoided in the control strategy.

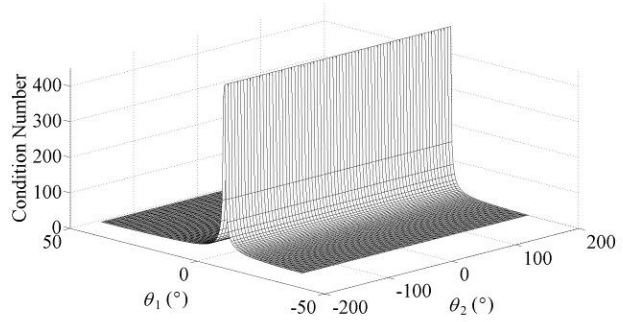

Figure 7. Condition number of the Jacobian matrix

To design a high-efficiency control strategy, we use two control modes. The first control mode, referred to as the direct control (or joint to joint control) mode, is used when θ_1 is close to 0 degree. Each of three motions of the game controller is mapped to a robot joint motion without kinematics calculation. In the second control mode, referred to as the kinematics control, we use kinematics for velocity control of the ureteroscope when the joystick moves left, right, up and down. Two buttons on the joystick are responsible for backward and forward movement. The value of θ_1 is used to determine which control mode is used. The kinematics control flow diagram is show in Fig. 8.

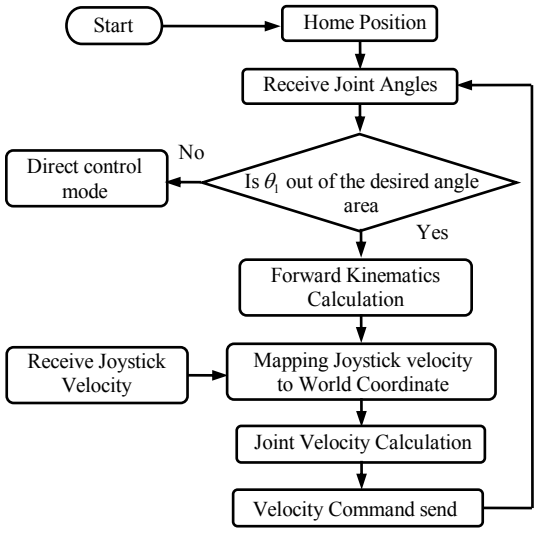

Figure 8. Kinematics control flow diagram

V. Experiment

We carried out the following two experiments to evaluate the system performance: a) comparative bladder phantom experiment; and b) phantom kidney experiment.

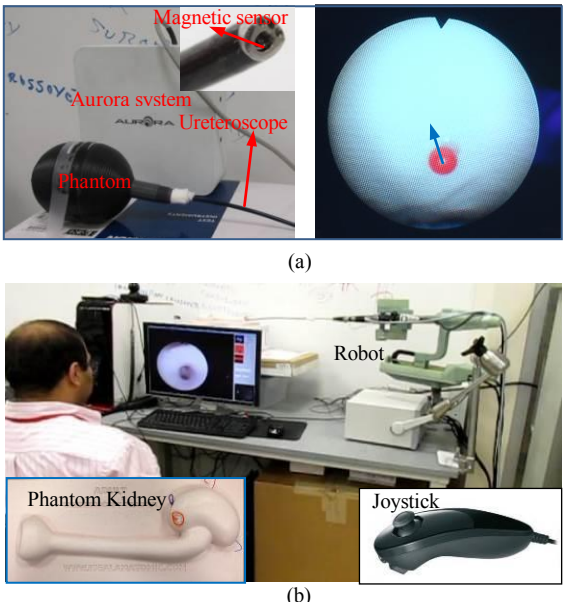

Figure 9. System experiment. (a) Comparation of robotic and manual procedure; (b) Robotic operation in phantom kidney system.

A. Comparative Bladder Phantom Experiment

In this experiment, we compared manual and robotic ureteroscopy operation. The experimental setup is shown in Fig. 9. A bladder phantom with four colored spherical targets of 4mm diameter was used. The ureteroscope was maneuvered in a specific order to each of the targets. The task

of reaching the target was completed when the target color filled the visual field of the ureteroscope. A 6 degrees-of-freedom electromagnetic sensor (Northern Digital, Waterloo, Canada) was inserted through the working channel to the ureteroscope tip for tracking purposes. The trajectories of the ureteroscope tip for the manual and robotic operation and the power spectral density diagrams are shown in Fig. 10.

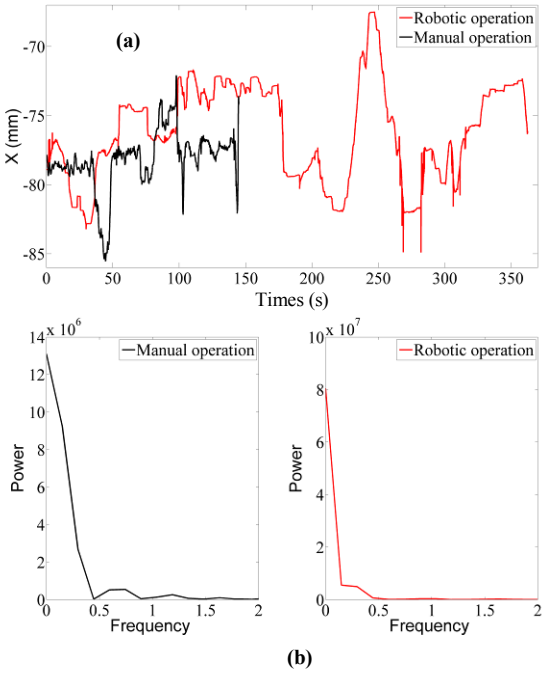

Figure 10. The trajectory of the ureteroscope in robotic and manual operation. (a) is tip position on x axis separately. (b) is power spectral density diagram.

Fig. 10 (a) shows the trajectories of the x co-ordinate of the ureteroscope tip for manual and robotic operation (the trajectories of the y and z co-ordinates are similar and not shown here). The total time for robotic operation was 362 seconds while that for manual operation was 145 seconds. To evaluate the trajectories for the two operations, we carried out a frequency domain analysis. Fig. 10 (b) shows the power spectral density for the two trajectories. We see from these plots that the amount of power present in the zero frequency component for robotic operation is 86.18% while it is only 47.31% for manual operation. Robotic operation is significantly smoother than manual operation and leads to a reduction in the non-zero component frequencies caused due to hand tremors and inexact maneuvers. However, the robotic operation needs more time than manual operation since in manual operation the ureteroscope can be moved quickly while the speed of the ureteroscope is limited on the robotic device. This can be improved in future designs.

B. Phantom Kidney Experiment

As shown in Fig. 9 (b), we used the robotic system to maneuver the ureteroscope to two targets in a kidney phantom. This experiment simulates a realistic renal collecting system and ureter. Two colored wires were inserted as task targets in the kidney phantom. An external sheath was used to support the flexible portion of the ureteroscope. During the experiment, the operator was able to successfully maneuver the ureteroscope through different sections of the phantom to both the targets. The ureteroscope movement was found to be smooth as seen from the ureteroscope tip trajectory. Furthermore, the ureteroscope video output was stable due to absence of hand tremors and inexact maneuvers.

VI. Conclusion

In this paper a robotic system was designed to control a 3-DOF flexible endoscope following the requirements developed by our clinical partners. The kinematics were analyzed considering the nonlinear flexion property and cable slack of the ureteroscope. To achieve more intuitive operation, the control combined kinematics and direct control mode. Initial experiments have shown the robot can smoothly and accurately drive the ureteroscope. The next step will be to go to animal tests and then pursue clinical trials.

References

[1] T. Yoshida, H. Inoue, Y. Kumagai, and T. Iwai, "Image-navigated endoscopic surgery: introduction of the face-mounted display system with picture-in-picture capabilities," *Hepatogastroenterology*, vol. 47, no. 32, pp. 375–377, Apr. 2000.

[2] A. S. Liberman, I. Shrier, and P. H. Gordon, "Injuries sustained by colorectal surgeons performing colonoscopy," *Surgical endoscopy*, vol. 19, pp. 1606-1609, Oct. 2005.

[3] P. Allemann, L. Ott, M. Asakuma et al., "Joystick Interfaces Are Not Suitable for Robotized Endoscope Applied to NOTES," *Surgical Innovation*, Vol.16 No. 2, pp. 111-116, Jun. 2009.

[4] K. Olds, A.T. Hillel, E. Cha, M. Curry, L.M. Akst, R.H. Taylor, and J.D. Richmon, "Robotic endolaryngeal flexible (Robo-ELF) scope: a preclinical feasibility study," *Laryngoscope*, vol. 121, no. 11, pp. 2371-4, Nov. 2011.

[5] C. A. Peters, A. Burns, E. Wilson, H. Luo, K. LeRoy, J. Goldie, B. LaBrecque, K. Cleary, "Navigated Endoscopy: Prototype System for Robotically Assisted Ureteroscopy," *The Hamlyn Symposium on Medical Robotics*, 72-74. 2012.

[6] M. M. Desai, R. Grover, M. Aron; A. Ganpule, S. S. Joshi, "Robotic Flexible Ureteroscopy for Renal Calculi: Initial Clinical Experience," *The Journal of Urology*, vol. 186, no. 2, pp. 563-568, Aug. 2011.

[7] J. Ruiter, E. Rozeboom, M. Van Der Voort, M. Bonnema, I. Broeders, "Design and evaluation of robotic steering of a flexible endoscope," Proc. *IEEE RAS and EMBS Int. Conf. on Biomedical Robotics and Biomechatronics*, pp. 761-767. 2012.

[8] J. Guo, S. Guo, N. Xiao and Y. Wang, " Development of Force Sensing Systems for a Novel Robotic Catheter System , " *Proc. IEEE Int. Conf. Robotics and Biomimetics (ROBIO)*, PP. 2213-2218. 2012

[9] C. Fang, W. Sang, J. D. J. Gumprecht, G. Strauss, T. C. Lueth, "Image-Guided Steering of a Motorized Hand-Held Flexible Rhino Endoscope in ENT Diagnoses", *Proc. IEEE Int. Conf. Robotics and Biomimetics (ROBIO)*, pp. 1086 - 1091. 2012

[10] H. S. Yoon, J. Jeon, J. H. Chung, B. J. Yi, "Error Compensation for a 2 DOF Bendable Endoscope Mechanism, " *13th International Conference on Control, Automation and Systems*, pp. 862-865. 2013

[11] P. M. Loschak, L. J. Brattain, and R. D. Howe, "Automated Pointing of Cardiac Imaging Catheters," *Proc. IEEE Int. Conf. Robotics and Automation*, pp. 5794 - 5799. 2013

[12] D.B. Camarillo; J.K. Salisbury; C.F. Milne; C.R.; Zinn M.R. Carlson, "Mechanics modeling of tendon-driven continuum manipulators," *IEEE Transactions on Robotics*, vol. 24, no. 6, pp.1262-1273, 2008.

[13] R. J. Webster III and B. A. Jones, "Design and kinematic modeling of constant curvature continuum robots: a review," *The International Journal of Robotics Research*, Vol. 29, No. 13, pp. 1661-1683. 2010.

[14] J. Angeles, *Fundamentals of Robotic Mechanical System, Theory, Methods, and Algorithms*. Spring-Verlag: New York, 2003.